The International Journal of Advanced Manufacturing Technology (2018) 99:2863–2875
https://doi.org/10.1007/s00170-018-2612-7

ORIGINAL ARTICLE

# Influence of chisel edge thinning on helical point micro-drilling performance

Haixin Guo[1] · Zhiqiang Liang[2] · Xibin Wang[2] · Tianfeng Zhou[2] · Li Jiao[2] · Longlong Teng[2] · Wenhua Shen[2]

Received: 12 May 2018 / Accepted: 16 August 2018 / Published online: 15 September 2018


## Abstract

Chisel edge thinning can effectively improve the drilling performance of austenitic stainless steel. Four kinds of helical point micro-drills, each with a thinned chisel edge of a distinct length, are fabricated based on the mathematics models of the micro-drill by using a six-axis computer numerical control tool grinder. Micro-drilling experiments on 304 stainless steel are conducted. Drilling performance is evaluated according to the measured and observed micro-hole machining quality, chip morphology, thrust force, and tool wear of the micro-drill tip. With a decrease in the chisel edge length, the micro-holes drilled using thinned micro-drills have small entrance burrs, roundness errors, and regular shapes, which are attributed to an increase in self-centering capability. Owing to increased equivalent chip thickness and different directions of chip flow, micro-drills with thinned chisel edge can generate more small-size chips and improve chip breaking. In addition, the inner cutting edge with a positive rake angle replaces the chisel edge with a negative rake angle to cut the workpiece, significantly reducing the chip curl, thrust force, and tool wear of micro-drills. However, helical point micro-drills with critical chisel edge lengths by thinning exhibit less thrust force and tool wear than do helical point micro-drills with no chisel edge because of the increase in the uncut chip width of the micro-drill. Thus, with the selected parameter range, the optimal helical point micro-drill is the micro-drill with a specific chisel edge length by thinning to improve drilling performance.

**Keywords** Chisel edge thinning · Stainless steel · Micro-drill · Drilling performance

## 1 Introduction

With the rapid development of science and technology, the application of micro-holes has become increasingly widespread. Micro-drilling is a predominant operation in micro-hole machining and has been widely applied in various fields, ranging from precision mechanics to advanced electronics [1]. These applications include the ejection nozzle of a diesel engine, as well as high-temperature and high-pressure components. These micro-hole components are often made of stainless steel because of the high strength, corrosion resistance, and high-temperature resistance of the material [2, 3]. However, during micro-drilling process of stainless steel, more than 50% of the drilling force produced by the chisel edge accelerates its wear, fracture, and breakage, thereby reducing its micro-drilling performance [4]. In addition, the

✉ Zhiqiang Liang
liangzhiqiang@bit.edu.cn

Haixin Guo
18811318020@163.com

Xibin Wang
cutting0@bit.edu.cn

Tianfeng Zhou
zhoutf@bit.edu.cn

Li Jiao
jiaoli@bit.edu.cn

Longlong Teng
313149334@qq.com

Wenhua Shen
7420161117@bit.edu.cn

[1] School of Mechanical Engineering, Beijing Institute of Technology, Beijing 100081, People's Republic of China

[2] Key Laboratory of Fundamental Science for Advanced Machining, Beijing Institute of Technology, Beijing 100081, People's Republic of China

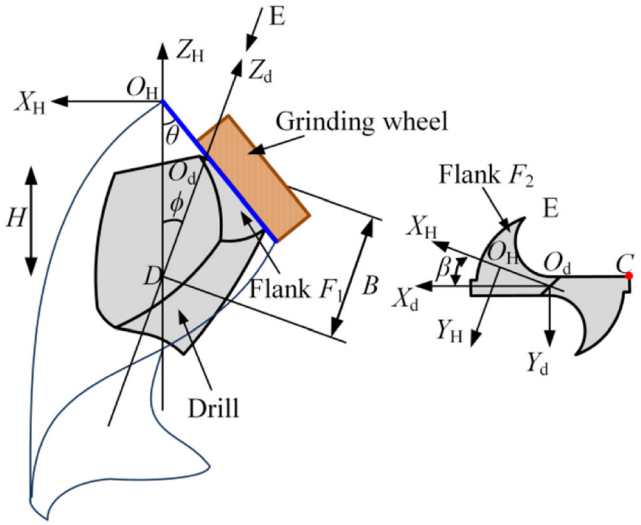


**Fig. 1** Mathematical model of flank surface

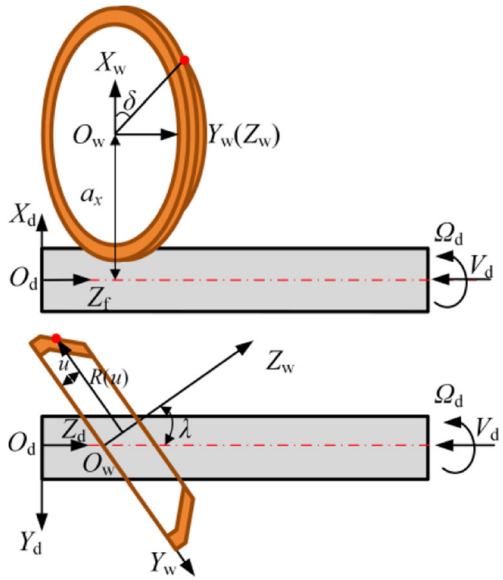


**Fig. 2** Mathematical model of the flute

poor self-centering capability of micro-drills with a small point angle severely affects the roundness and hole-wall machining quality.

Chisel edge thinning of micro-drills can noticeably improve self-centering capability and reduce drilling force. Pre-thinned designs reported in the literature include the split drill point [5], linear-notch design [6, 7], and circular-notch design [8]. Development of pre-thinned designs is expected to continue as published results indicate that efficient pre-thinning significantly improves drilling performance. Wang X et al. [9] drilled printed circuit board (PCB) through-holes by regular drill and thinned drill; the results indicated that appropriate thinning of the chisel edge contributes to flank wear reduction, but exerts no apparent effect on burr size reduction for PCB through-hole drilling. During the drilling process of lead-free brass, Kato H et al. [10] found that web thinning reduces thrust force by using low-stiffness micro-drills with a diameter of 0.2 mm. Nanbu Y et al. [11, 12] revealed that thinning of micro-drills with diameters of 0.1 mm and 0.2 mm led to a reduction in thrust force. The optimal rank angle of the chisel edge in tool life ranged from −10° to 0°. On the basis of the position of the grinding wheel, Lin P. D et al. [13] proposed a method for the accurate fabrication of two-flute twist drills by thinning. The drilling experiment confirmed that thinning can be a valuable method for improving drilling performance.

The helical point micro-drill can improve the drilling performance compared with planar and conical drill points [14, 15]. However, studies have been rarely reported on the micro-drilling performance of a helical point micro-drill with a thinned chisel edge, particularly the helical point micro-drill with a diameter of less than 0.5 mm. Chisel edge thinning of a helical point micro-drill also involves complexity, with dimensional and shape accuracy requirements that are difficult to meet.

Therefore, the current study analyzes the effect of the chisel edge thinning of a helical point micro-drill on the drilling performance of stainless steel. Based on the mathematical models of the helical point micro-drill, the rake angle, lip inclination angle, uncut chip thickness, uncut chip width, and cutting edge shape are calculated with the MATLAB software. Four kinds of helical point micro-drills, each with a

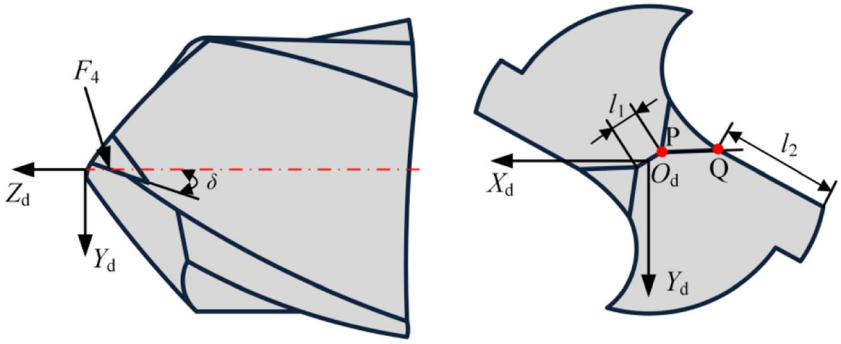


**Fig. 3** Mathematical model of the thinned chisel edge of the helical point drill

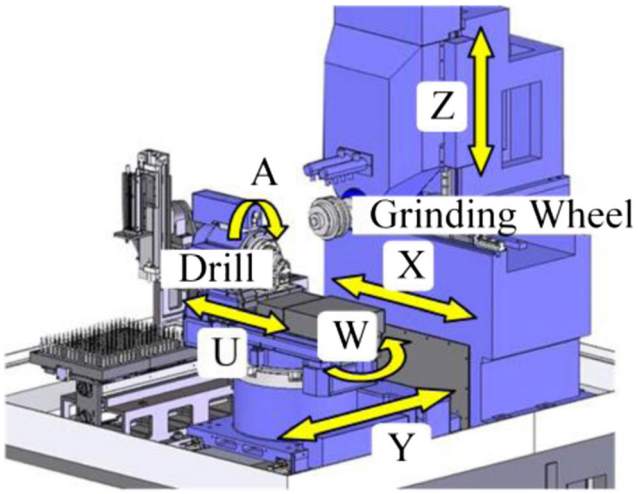


**Fig. 4** Six-axis CNC grinding machine

thinned chisel edge of a distinct length, are fabricated using a six-axis computer numerical control (CNC) grinding machine. Micro-drilling experiments on 304 stainless steel are conducted. The chip morphology, thrust force, tool wear, and quality of micro-holes are measured and observed. The helical point micro-drill with optimal chisel edge length by thinning is determined from the results.

## 2 Mathematical model of the helical point micro-drill

### 2.1 Mathematical model of the helical flank of the helical point micro-drill

Based on the mathematical model proposed by Liang [16], the mathematical model of the helical flank surface of the micro-drill is shown in Fig. 1. The $O_H$-$X_HY_HZ_H$ system and $O_w$-$X_wY_wZ_w$ system are the coordinate frame of the helical surface and grinding wheel, respectively. The $O_d$-$X_dY_dZ_d$ system is the micro-drill coordinate system, where the coordinate origin $O_d$ is located at the center of the micro-drill tip; the $Z_d$-axis coincides with the micro-drill axis; and the direction of the $X_d$-axis and the $Y_d$-axis enables the $y$-coordinate of the outer corner C on the main cutting edge to satisfy the equation $y_c = -t$ ($2t$ is web thickness). The equation of the helical flank in the $O_d$-$X_dY_dZ_d$ system can be expressed as follows:

$$F_1 : Z_d\cos\phi - B\frac{\sin\phi}{\tan\theta} + X_a\sin\phi + \frac{\sqrt{[X_a\cos\phi - \sin\phi(Z_d + B)]^2 + {Y_a}^2}}{\tan\theta} + \frac{H}{2\pi}\arcsin\left(\frac{Y_a}{\sqrt{[X_a\cos\phi - \sin\phi(Z_a + B)]^2 + {Y_a}^2}}\right) = 0 \quad (1)$$

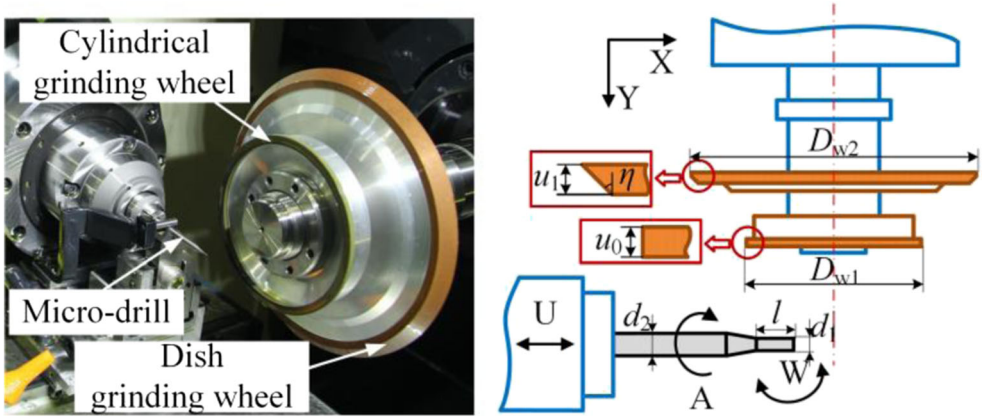


**Fig. 5** Geometry and configuration of the grinding wheels

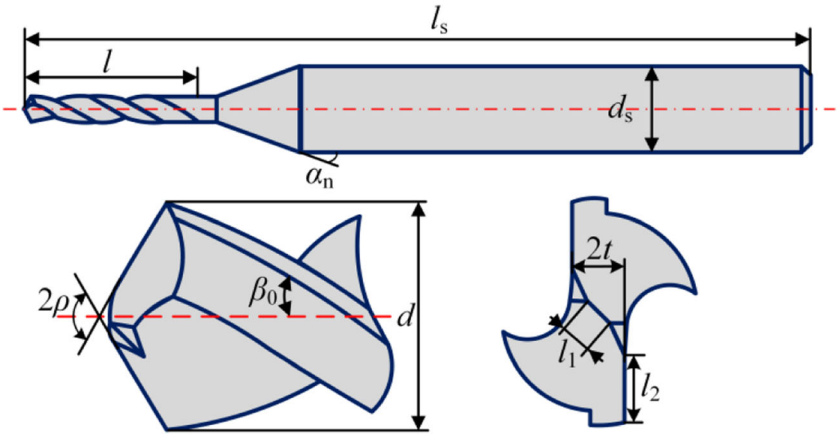


**Fig. 6** Structure of the micro-drill

**Table 1** Geometric parameters of the helical point micro-drill

| No. | | 1 | 2 | 3 | 4 |
|---|---|---|---|---|---|
| Chisel edge length $l_1$ (μm) | | 0 | 42 | 84 | 140 |
| Length of the main cutting edge $l_2$ (μm) | | 196 | 196 | 196 | 207 |
| Drill diameter $d$ (mm) | 0.5 | Axial rank angle $\delta$ (°) | 0 | Flute length $l$ (mm) | 1.5 |
| Drill whole length $l_s$ (mm) | 50 | Web thickness $2t$ (μm) | 125 | Helix angle $\beta_0$ (°) | 30 |
| Drill shank diameter $d_s$ (mm) | 3 | Drill neck angle $\alpha_n$ (°) | 10 | Point angle $2\rho$ (°) | 118 |

where $X_a = X_d \cos\beta - Y_d \sin\beta$, $Y_a = Y_d \cos\beta + X_d \sin\beta$, and $\theta$, $\beta$, $\phi$, $B$, and $H$ are the grinding parameters of the helical flank.

Substituting $X'_d = -X_d$, $Y'_d = -Y_d$, and $Z'_d = Z_d$ into Eq. (1), the mathematical model of the helical flank $F_2(X'_d, Y'_d, Z'_d) = 0$ can be accordingly obtained. In addition, the relationship between drill geometry parameters ($\rho$, $\psi$, $\alpha_{fc}$, $\alpha^r$ h,-60°) and grinding parameters ($\theta$, $\beta$, $\phi$, $B$, $H$) is derived as follows [17]:

$$\begin{cases} \rho = g_1(\theta,\ \beta,\ \phi,\ B,\ H) \\ \psi = g_2(\theta,\ \beta,\ \phi,\ B,\ H) \\ \alpha_{fc} = g_3(\theta,\ \beta,\ \phi,\ B,\ H) \\ \alpha^{r}_{h,-60^\circ} = g_4(\theta,\ \beta,\ \phi,\ B,\ H) \end{cases} \tag{2}$$

where $2\rho$ is the point angle, $\psi$ is the chisel edge angle, $\alpha_{fc}$ is the lip clearance angle, and $\alpha^r$ h,-60° is the heel clearance angle.

## 2.2 Mathematical model of the micro-drill flute of the helical point micro-drill

Based on the micro-drill flute mathematical model proposed by Zhang [18], the grinding process of the micro-drill flute is illustrated in Fig. 2. The micro-drill flute is generated by the relative spiral motion between the grinding wheel and the micro-drill. The rotational movement of the grinding wheel around its axis constitutes a main cutting movement, and the micro-drill rotates and moves around its axis at $\Omega_d$ and $V_d$ to constitute a spiral movement. The cutting path can be derived as follows:

$$\boldsymbol{R}_m(u,\delta) = \begin{bmatrix} X_{Pm}(u,\delta) \\ Y_{Pm}(u,\delta) \end{bmatrix} = \begin{bmatrix} X_{Pf}\cos(-Z_{Pf}\tan(\beta_0)/r) - Y_{Pf}\sin(-Z_{Pf}\tan(\beta_0)/r) \\ X_{Pf}\sin(-Z_{Pf}\tan(\beta_0)/r) + Y_{Pf}\cos(-Z_{Pf}\tan(\beta_0)/r) \end{bmatrix} \tag{3}$$

where $[X_{Pf}\ \ Y_{Pf}\ \ Z_{Pf}] = [R(u)\cos\delta + a_x\ \ R(u)\sin\delta\cos\lambda - u\sin\lambda\ \ R(u)\sin\delta\sin\lambda + u\cos\lambda]$, $u$ and $\delta$ are the parameters of the wheel profile, $a_x$ and $\lambda$ are the parameters of the wheel position, $r$ is the micro-drill radius, and $\beta_0$ is the helix angle.

The coordinate points of the flute profile are processed by cubic spline interpolation, and the equation of the cross-section profile of the drill flute is expressed as $y_d = f_H(x_d)$. The spiral groove surface is formed by the helical motion of the cross-section profile; thus, the mathematical model of the drill flute in the $O_d$-$X_dY_dZ_d$ system is expressed as follows:

$$F_3 : \begin{cases} X_d = w\cos v - f_H(w)\sin v \\ Y_d = w\sin v + f_H(w)\cos v \\ Z_d = z_c + rv/\tan\beta_0 \end{cases} \tag{4}$$

where $w$ and $v$ are the variable parameters to generate the flute surface, and $z_c$ is the $z$-coordinate value of the outer corner C in the $O_d$-$X_dY_dZ_d$ system.

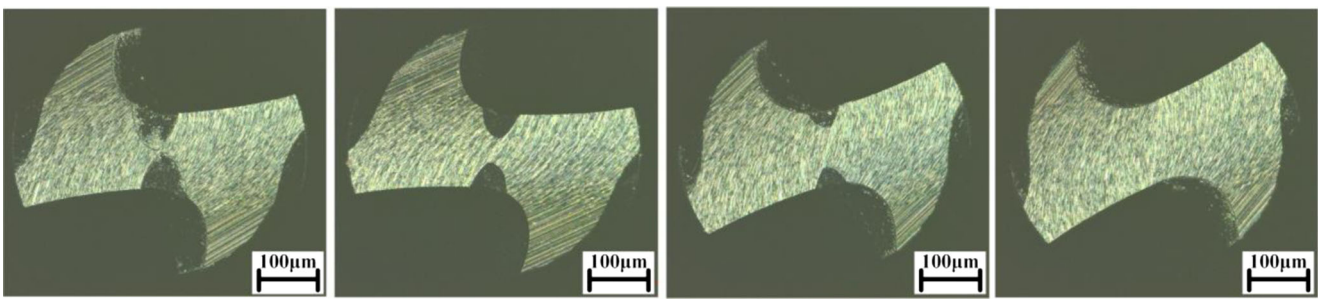


(a) Tool 1($l_1$=0 μm) (b) Tool 2($l_1$=42 μm) (c) Tool 3($l_1$=84 μm) (d) Tool 4($l_1$=140 μm)

**Fig. 7** Grinding experiment results for the helical point micro-drills. **a** Tool 1 ($l_1 = 0$ μm). **b** Tool 2 ($l_1 = 42$ μm). **c** Tool 3 ($l_1 = 84$ μm). **d** Tool 4 ($l_1 = 140$ μm)

### 2.3 Mathematical model of the thinned chisel edge of the helical point micro-drill

The mathematical model of the chisel edge $L_0(X_d, Y_d, Z_d) = 0$ obtained using the simultaneous flank equations Eqs. (1)–(2) is derived as follows:

$$L_0 : 2X_a\sin\phi + \frac{\sqrt{[X_a\cos\phi - \sin\phi(Z_d + B)]^2 + {Y_a}^2} - \sqrt{[X_a\cos\phi + \sin\phi(Z_d + B)]^2 + {Y_a}^2}}{\tan\theta} + \frac{H}{2\pi}\left\{\arcsin\left(\frac{Y_a}{\sqrt{[X_a\cos\phi - \sin\phi(Z_d + B)]^2 + {Y_a}^2}}\right) + \arcsin\left(\frac{Y_a}{\sqrt{[X_a\cos\phi + \sin\phi(Z_d + B)]^2 + {Y_a}^2}}\right)\right\} = 0 \quad (5)$$

In the $O_d$-$X_dY_dZ_d$ system, the mathematical model of the thinned chisel edge is presented in Fig. 3. The rake face $F_4$ is a plane, intersecting the chisel edge at point $P$ ($x_p$, $y_p$, $z_p$) and the main cutting edge at point $Q$ ($x_q$, $y_q$, $z_q$). Thus, the line $PQ$ is the inner cutting edge. The length of the chisel edge is denoted by $l_1$, and the length of the main cutting edge is denoted by $l_2$. The axial rake angle is $\delta$. The mathematical model of the rank face $F_4(X_d, Y_d, Z_d) = 0$ obtained using the chisel edge equation Eq. (5) is derived as follows:

$$F_4 : aX_d + bY_d + cZ_d + d = 0 \quad (6)$$

where $a$, $b$, $c$, and $d$ are determined by $L_1$, $L_2$, and $\delta$.

## 3 Grinding experiment of helical point micro-drills with thinned chisel edge

Based on mathematical models of the helical point micro-drill with a thinned chisel edge, helical point micro-drills are fabricated using a six-axis CNC grinding machine (CNS7d; Makino Seiki Co., Ltd.), as shown in Fig. 4. During the grinding process of micro-drills, its shank is clamped on the $A$-axis; the micro-drill can also move along the $U$-axis and $Y$-axis, as well as rotate about the $W$-axis. The grinding wheel can move along the $X$-axis and $Z$-axis. The grinding process of the helical point micro-drill with a thinned chisel edge includes helical flank grinding, drill flute grinding, and chisel edge thinning; it also uses two types of grinding wheels. The geometry parameters of the configuration of the grinding wheels are shown in Fig. 5. The helical flank is ground by cylindrical grinding wheel with $D_{w1} = 80$ mm, and $u_0 = 3$ mm. The micro-drill flute and thinned chisel edge are ground by a dish grinding wheel with $D_{w2} = 135$ mm, $u_1 = 4$ mm, and $\eta = 45°$.

To analyze the influence of chisel edge length by thinning on micro-drilling performance, four kinds of helical point micro-drills—each with a thinned chisel edge of a distinct length—are fabricated. The structure of the micro-drill is presented in Fig. 6, and the geometric parameters are listed in Table 1. The results for the fabricated micro-drills are shown in Fig. 7.

## 4 Drilling experiment using helical point micro-drill with thinned chisel edge

Micro-drilling experiments using different helical point micro-drills are conducted on a DMG machining center

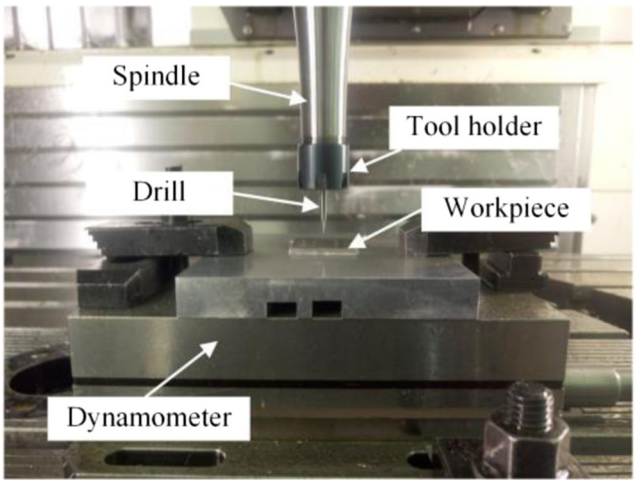


**Fig. 8** Drilling experiment setup on the DMG machining center

(DMU80 monoBLOCK; DMG MORI Co., Ltd.), as shown in Fig. 8. The workpiece material is 304 austenitic stainless steel. The drilling force is measured using a Kistler piezoelectric dynamometer model 9257B. The tool wear, hole quality, and chip morphology are measured using a 3D laser scanning microscope (VK-X100; Keyence Co., Ltd.) and a zoom-stereo microscope (V12; Zeiss Co., Ltd.).

### 4.1 Chip morphology of helical point micro-drills with thinned chisel edge

The chip morphology of helical point micro-drills with thinned chisel edge under rotational speed $n = 14{,}000$ r/min and feed per tooth $f_z = 14$ mm/min is shown in Fig. 9. Chip curl occurs and becomes more apparent from tool 1 ($l_1 =$

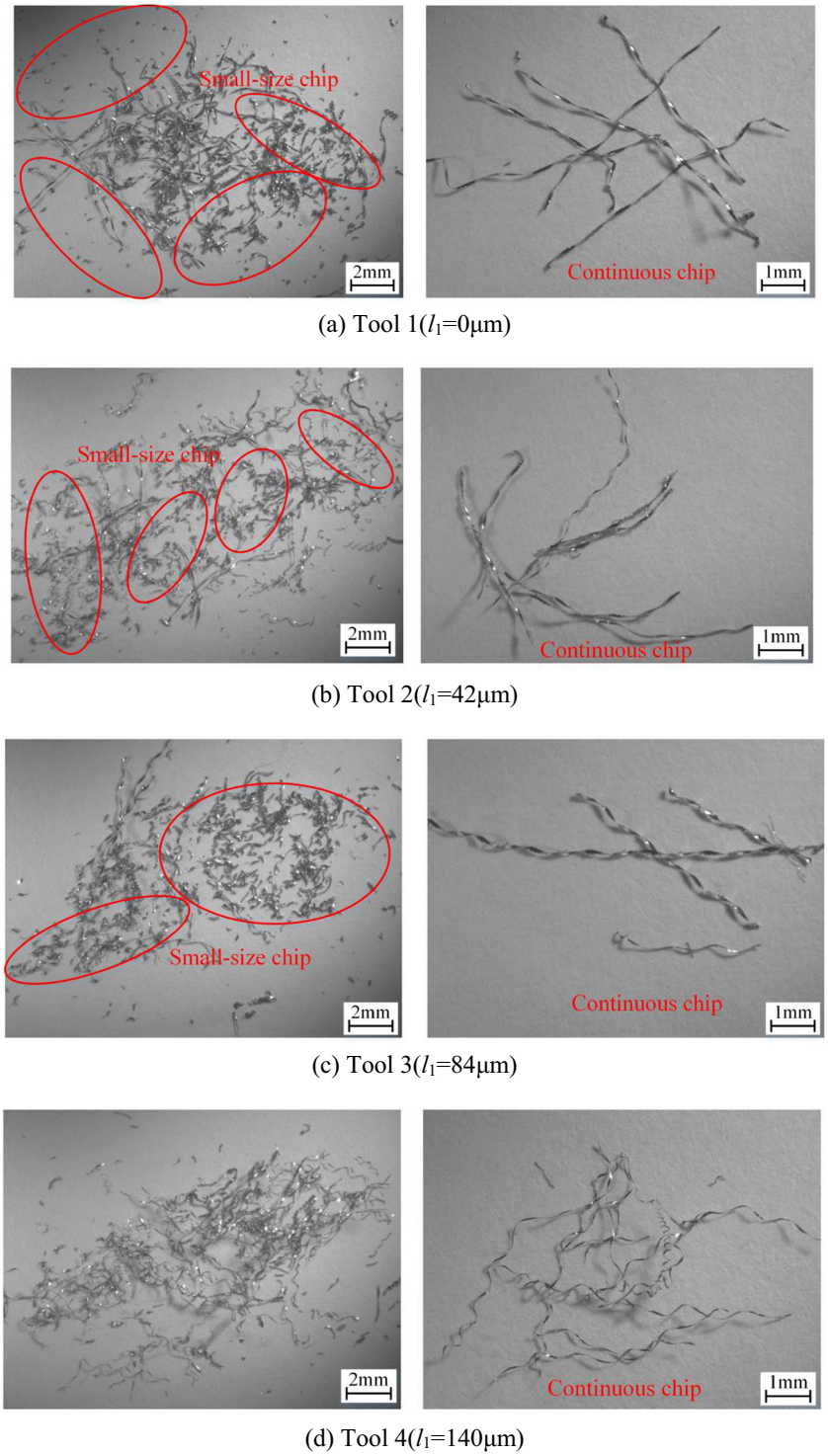


**Fig. 9** Chip morphology of the micro-drills with thinned chisel edge. **a** Tool 1 ($l_1 = 0$ μm) **b** Tool 2 ($l_1 = 42$ μm). **c** Tool 3($l_1 =$ 84 μm). **d** Tool 4 ($l_1 = 140$ μm)

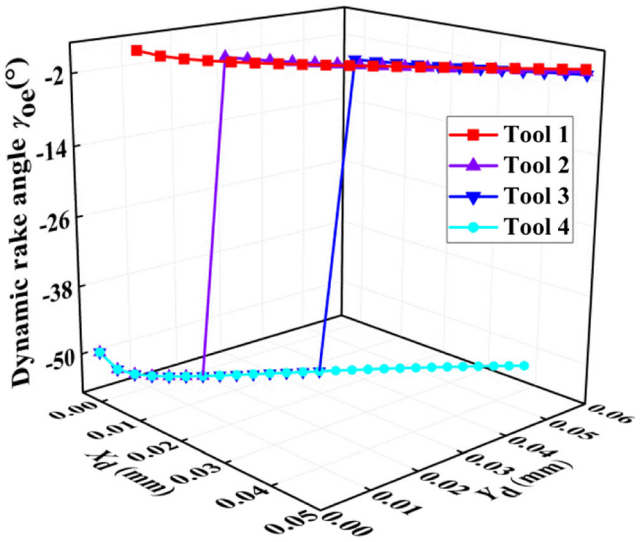


Fig. 10 Dynamic rake angle

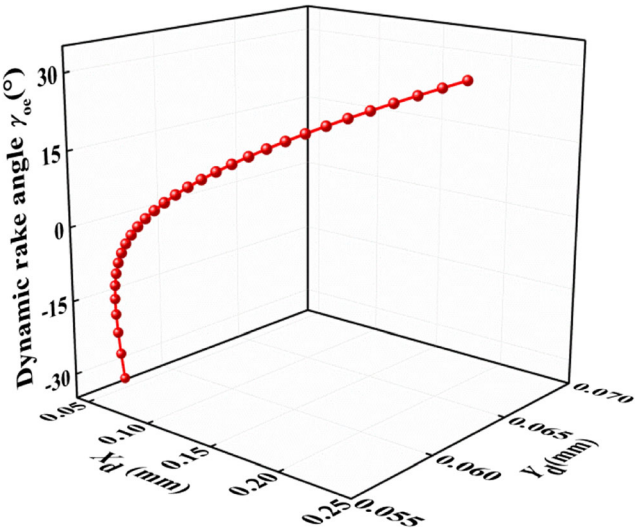


Fig. 13 Dynamic rank angle along the main cutting lip

0 μm) to tool 4 ($l_1$ = 140 μm). Moreover, the chip morphology of tool 4 ($l_1$ = 140 μm) is basically a long and continuous chip, which easily wraps around the micro-drill body, thus hindering chip removal. The chips produced by thinned micro-drills are segmented to a shorter length and even to small pieces.

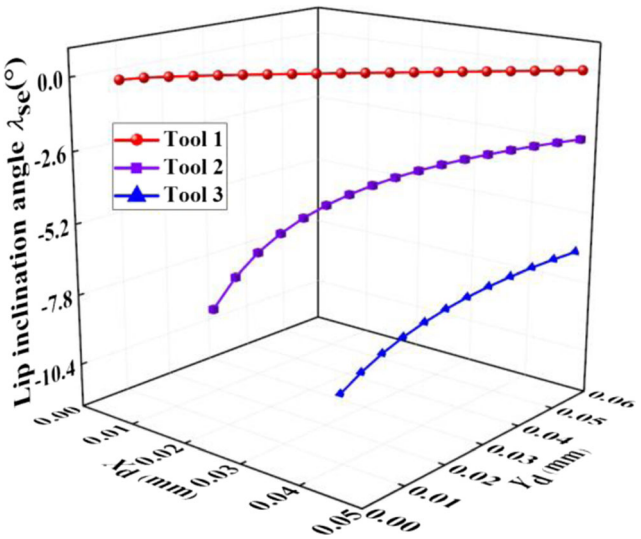


Fig. 11 Dynamic lip inclination angle

Tool 1 ($l_1$ = 0 μm), tool 2 ($l_1$ = 42 μm), and tool 3 ($l_1$ = 84 μm) generate a large number of small-size chips, and a small number of continuous chips, resulting in an increase in chip removal. The proportion of small-size chips increases with an increase in chisel edge length.

Chip curl depends on the working angle along the cutting lip, with the lip inclination angle $\lambda_{se}$ and rake angle $\gamma_{oe}$ as the main influencing factors. The lip inclination angle $\lambda_{se}$ along the cutting edge affects chip curl and flow, whereas the lip inclination angle $\lambda_{se}$ along the chisel edge has almost no effect on the same. The rake angle $\gamma_{oe}$ influences the degree of chip deformation. The chip compression ratio $\Lambda_h$ can be expressed as $\Lambda_h = \cos(\phi - \gamma_{oe})/\sin\phi$, where $\phi = \pi/4 - (\beta_f - \gamma_{oe})$, $\phi$ is the shear angle, and $\beta_f$ is the frictional angle. Thus, the rake angle $\gamma_{oe}$ significantly affects the chip compression ratio $\Lambda_h$.

According to the calculation method proposed by Zhang [18], the calculated result of the dynamic rake angle $\gamma_{oe}$ along the drill tips of micro-drills with $f_z$ = 14 mm/min is shown in Fig. 10; and the dynamic lip inclination angle $\lambda_{se}$ along the inner cutting edge of tool 1 ($l_1$ = 0 μm), tool 2 ($l_1$ = 42 μm), and tool 3 ($l_1$ = 84 μm) with $f_z$ = 14 mm/min is shown in Fig. 11. With a gradual increase in chisel edge lengths, the chisel edge with a negative rake angle replaces the inner cutting edge with a positive rake angle to squeeze the workpiece,

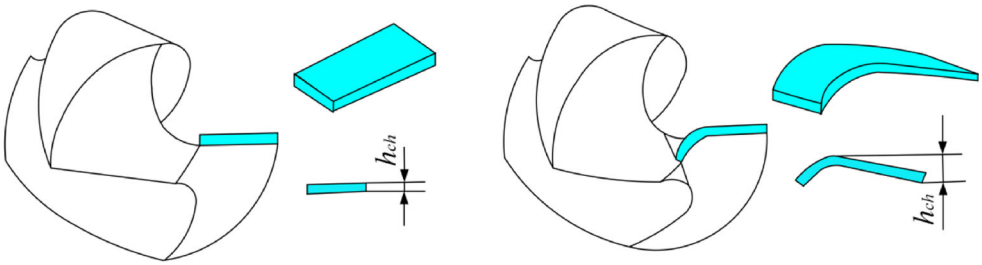


(a) Normal micro-drill (b) Micro-drill with thinned chisel edge

Fig. 12 Equivalent cutting thickness of the micro-drills. **a** Normal micro-drill. **b** Micro-drill with thinned chisel edge

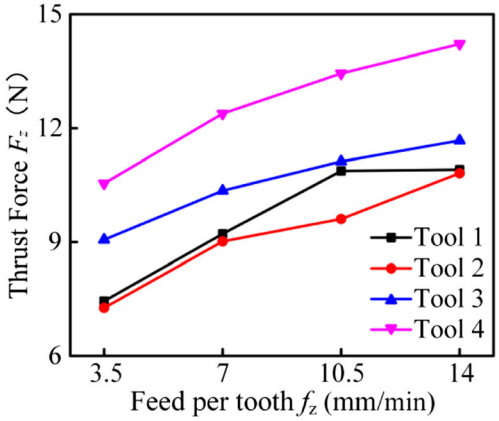


**Fig. 14** Average thrust force of two micro-holes with feed per tooth

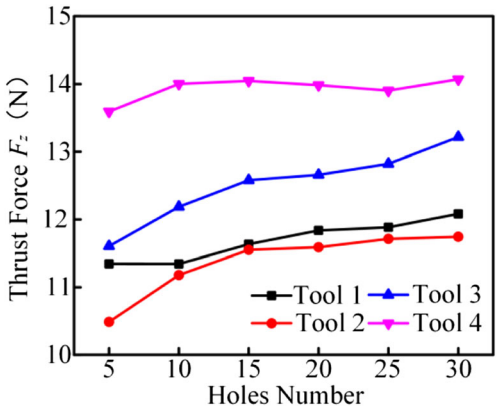


**Fig. 15** Thrust force with holes' number under feed per tooth $f_z = 14$ mm/min

thereby increasing the degree of chip deformation. Moreover, the increase in the negative value of the lip inclination angle from tool 1 ($l_1 = 0$ μm) to tool 3 ($l_1 = 84$ μm) further intensifies the chip curl.

The equivalent cutting thickness of the helical point micro-drill is shown in Fig. 12. The original section of a chip produced using a regular micro-drill (tool 4) is a rectangle, and the equivalent chip thickness $h_{ch}$ is relatively small, resulting in the relative difficulty of chip breaking. The profiles of the chips produced using tool 1 ($l_1 = 0$ μm), tool 2 ($l_1 = 42$ μm), and tool 3 ($l_1 = 84$ μm) generate an arc. The equivalent chip thickness $h_{ch}$ and the bending moment are increased, which contribute to chip breaking. The calculated result of the dynamic rake angle $\gamma_{oe}$ along the main cutting edge is shown in Fig. 13. The rake angle between the main cutting edge and the inner cutting edge has a larger difference; thus, the direction of the chip flow is different. The internal stress between two pieces of chips causes additional strain on the chip, which also contributes to chip breaking. Thus, the chips of tool 1 ($l_1 = 0$ μm), tool 2 ($l_1 = 42$ μm), and tool 3 ($l_1 = 84$ μm) have numerous small-size chips compared with tool 4 ($l_1 = 140$ μm). Owing to the decrease in the inner cutting edge, the proportion of small-size chips increases from tool 1 ($l_1 = 0$ μm) to tool 3 ($l_1 = 84$ μm).

### 4.2 Drilling force of helical point micro-drill with thinned chisel edge

Drilling experiments are conducted under rotational speed $n = 14{,}000$ r/min and feed per tooth $f_z = 3.5$, 7, 10.5, 14 mm/min. The average thrust force of the helical

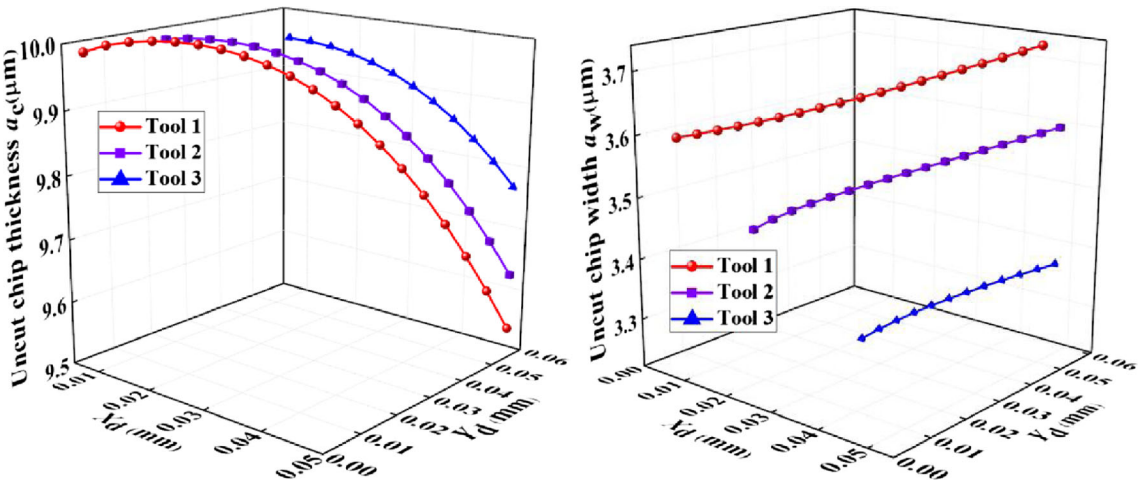


(a) Uncut chip thickness (b) Uncut chip width

**Fig. 16** Uncut chip thickness and uncut chip width along the inner cutting edge of tools 1, 2, and 3 with $f_z = 14$ mm/min. **a** Uncut chip thickness. **b** Uncut chip width

point micro-drill with thinned chisel edge is shown in Fig. 14. The thrust force is basically proportional to the feed per tooth. Compared with tool 4 ($l_1 = 140$ μm), the thrust force of tool 1 ($l_1 = 0$ μm), tool 2 ($l_1 = 42$ μm), and tool 3 ($l_1 = 84$ μm) are significantly reduced. When the feed per tooth $f_z$ is 14 mm/min, tool 1 ($l_1 = 0$ μm), tool 2 ($l_1 = 42$ μm), tool 3 ($l_1 = 84$ μm), and tool 4 ($l_1 = 140$ μm) each has a thrust force of 10.91, 10.81, 11.68, and 14.22 N, respectively. Compared with that of tool 4 ($l_1 = 140$ μm), the thrust force of each of tool 1 ($l_1 = 0$ μm), tool 2 ($l_1 = 42$ μm), and tool 3 ($l_1 = 84$ μm) is reduced by 23.28%, 23.98%, and 17.86%, respectively. The average thrust force of the micro-drill with varying number of holes and under rotational speed $n = 14{,}000$ r/min and feed per tooth $f_z = 14$ mm/min is shown in Fig. 15. The thrust force rises linearly as the number of

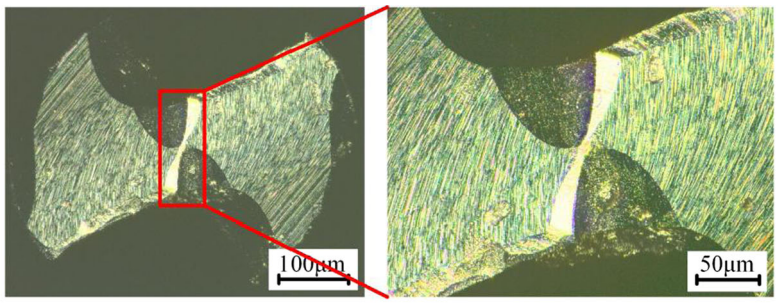


(a) Tool 1($l_1$=0 μm)

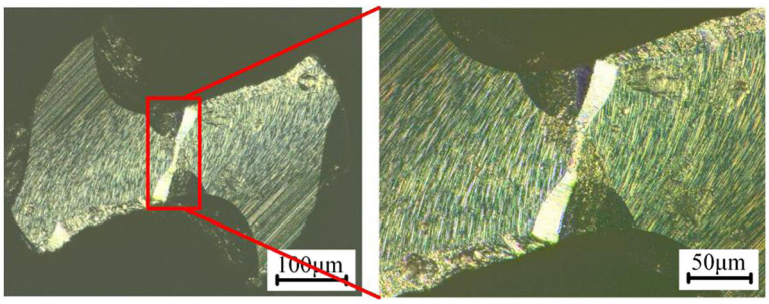


(b) Tool 2($l_1$=42 μm)

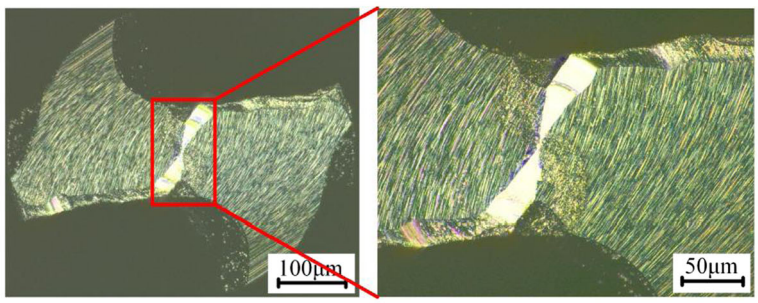


(c) Tool 3($l_1$=84 μm)

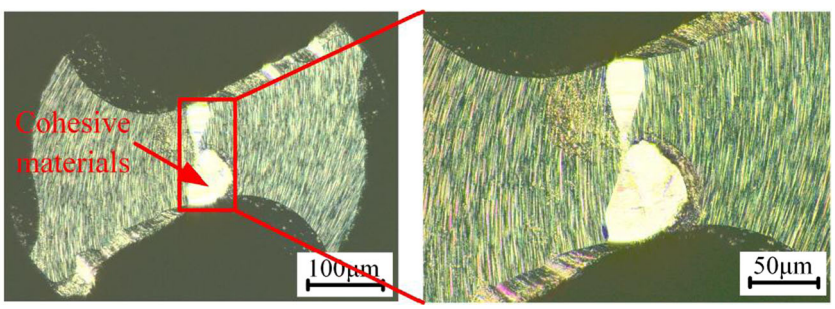


(4) Tool 4($l_1$=140 μm)

**Fig. 17** Microscope photograph of drill tip wear of helical point micro-drills with thinned chisel edge. **a** Tool 1 ($l_1 = 0$ μm). **b** Tool 2 ($l_1 = 42$ μm). **c** Tool 3 ($l_1 = 84$ μm). **d** Tool 4 ($l_1 = 140$ μm)

holes increases. The thrust force is reduced significantly from tool 4 ($l_1 = 140$ μm) to tool 2 ($l_1 = 42$ μm); however, the thrust force of tool 1 ($l_1 = 0$ μm) is slightly greater than that of tool 2 ($l_1 = 42$ μm).

The length of the thinned chisel edge considerably affects the rake angle, uncut chip thickness, and uncut chip width, which finally has also an effect on the drilling force. The uncut chip thickness and uncut chip width along the inner cutting edge of tool 1 ($l_1 = 0$ μm), tool 2 ($l_1 = 42$ μm), and tool 3 ($l_1 = 84$ μm) are shown in Fig. 16. With a gradual increase in chisel edge lengths, the chisel edge with negative rake angle is considered to squeeze workpiece, instead of the inner cutting edge with positive rake angle. Consequently, the thrust force from tool 2 ($l_1 = 42$ μm) to tool 4 ($l_1 = 140$ μm) increases. However, for the helical point micro-drills with no chisel edge, the uncut chip width of the inner cutting edge is increased, resulting in a slight increment in thrust force relative to the thrust force of tool 2 ($l_1 = 42$ μm).

### 4.3 Wear of helical point micro-drills with thinned chisel edge

Under rotational speed $n = 14{,}000$ r/min and feed per tooth $f_z = 14$ mm/min, four kinds of helical point micro-drills with thinned chisel edge are used to perform the micro-drilling tests. Drill wear is measured and analyzed using a 3D laser scanning microscope (VK-X100 by Keyence Co., Ltd.). After drilling 30 holes, a microscope photograph showing the wear of helical point micro-drills with a thinned chisel edge and the magnification of drill tip wear are presented in Fig. 17. Drill tip wear is apparent for the four kinds of micro-drills. The outer corner of the inner cutting edge exhibits the most wear, and the wear width gradually decreases from the outer corner to the center of the drill tip. Moreover, the drill tip wear of tool 1 ($l_1 = 0$ μm), tool 2 ($l_1 = 42$ μm), and tool 3 ($l_1 = 84$ μm) is less than that of tool 4 ($l_1 = 140$ μm), and the workpiece material sticks to the flank of tool 4 ($l_1 = 140$ μm).

To quantificationally analyze the degree of wear of the micro-drill tip, the wear width of the inner cutting edge $C_{max}$ is measured, and the method of wear measurement is shown in Fig. 18. The $C_{max}$ value of the inner cutting edge wear is shown in Fig. 19. The inner cutting edge wear of tool 4 ($l_1 = 140$ μm) is greater than those of other micro-drills. Thrust force plays an important role in micro-drill wear; thus, tool 2 ($l_1 = 42$ μm) has the least inner cutting edge wear $C_{max}$ because of less drilling force which is also influenced by tool wear.

### 4.4 Hole machining quality of helical point micro-drills with thinned chisel edge

The morphology of micro-hole entrance produced using tool 1 ($l_1 = 0$ μm), tool 2 ($l_1 = 42$ μm), tool 3 ($l_1 = 84$ μm), and tool 4

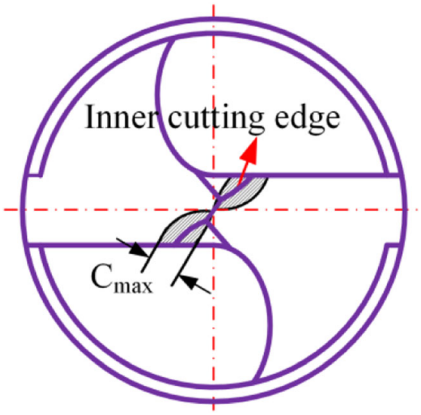


**Fig. 18** Schematic of wear measurement

($l_1 = 140$ μm) is presented in Fig. 20. As the number of micro-holes increases, the shape accuracy at the micro-hole entrance gradually decreases. The micro-holes produced using tool 1 ($l_1 = 0$ μm), tool 2 ($l_1 = 42$ μm), and tool 3 ($l_1 = 84$ μm) have small entrance burrs and regular shapes, and the 30 micro-holes produced using tool 4 ($l_1 = 140$ μm) have more entrance burrs. The roundness of the micro-holes is measured using a 3D laser scanning microscope (Keyence VK-X100). The method of roundness measurement is illustrated in Fig. 21. Roundness is the error between the incircle radius $R_1$ and the circumcircle radius $R_2$. Figure 22 shows the roundness value of the micro-holes drilled using tool 1 ($l_1 = 0$ μm), tool 2 ($l_1 = 42$ μm), tool 3 ($l_1 = 84$ μm), and tool 4 ($l_1 = 140$ μm). The roundness value increases with an increase in the number of micro-holes, and the roundness of micro-holes from tool 1 ($l_1 = 0$ μm) to tool 4 ($l_1 = 140$ μm) gradually increases.

The morphology of the micro-hole entrance depends on the self-centering ability. The shape of micro-drill tip is shown in Fig. 23. The self-centering capability of the micro-drills from tool 1 ($l_1 = 0$ μm) to tool 4 ($l_1 = 140$ μm) gradually decreases owing to an increase in the point angle of the micro-drill tip, resulting in a gradual increase in the roundness error of the micro-holes from tool 1 ($l_1 = 0$ μm) to tool 4 ($l_1 = 140$ μm). The cutting edge wear discussed in Section 4.3 plays an

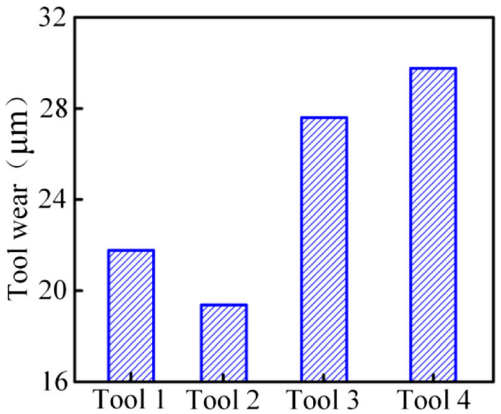


**Fig. 19** Wear of the inner cutting edge

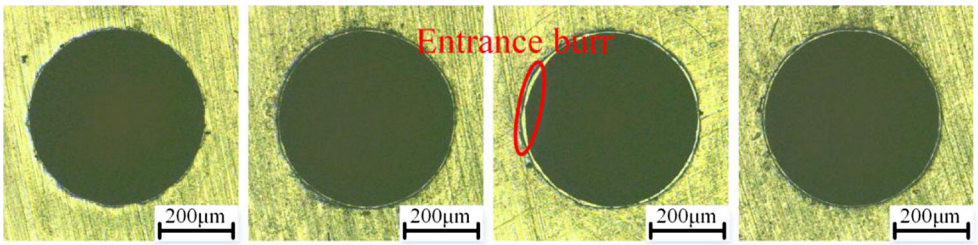


(a) The 1st, 10th, 20th, and 30th micro-holes drilled using Tool 1($l_1$=0 μm)

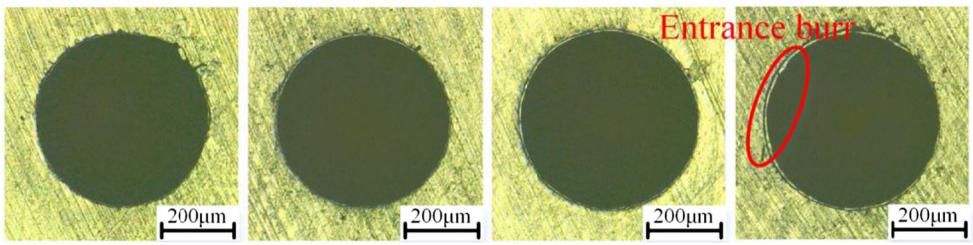


(b) The 1st, 10th, 20th, and 30th micro-holes drilled using Tool 2($l_1$=42 μm)

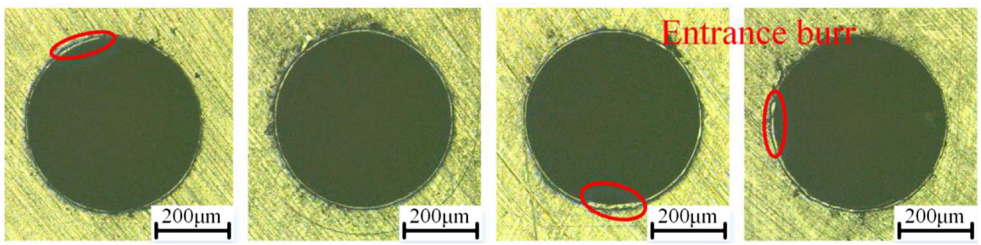


(c) The 1st, 10th, 20th, and 30th micro-holes drilled using Tool 3($l_1$=84 μm)

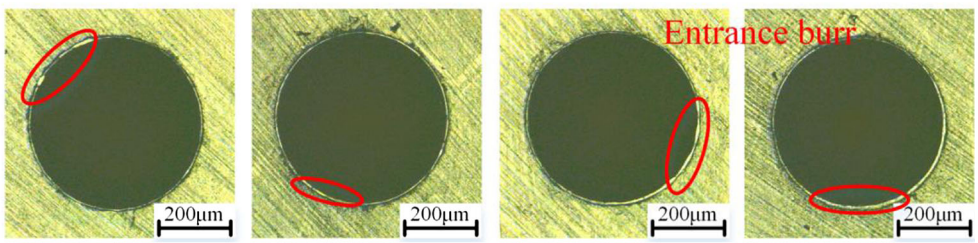


(d) The 1st, 10th, 20th, and 30th micro-holes drilled using Tool 4($l_1$=140 μm)

**Fig. 20** Micro-holes produced using the micro-drill with thinned chisel edge. **a** The 1st, 10th, 20th, and 30th micro-holes drilled using tool 1 ($l_1$ = 0 μm). **b** The 1st, 10th, 20th, and 30th micro-holes drilled using tool 2 ($l_1$ = 42 μm). **c** The 1st, 10th, 20th, and 30th micro-holes drilled using tool 3 ($l_1$ = 84 μm). **d** The 1st, 10th, 20th, and 30th micro-holes drilled using tool 4 ($l_1$ = 140 μm)

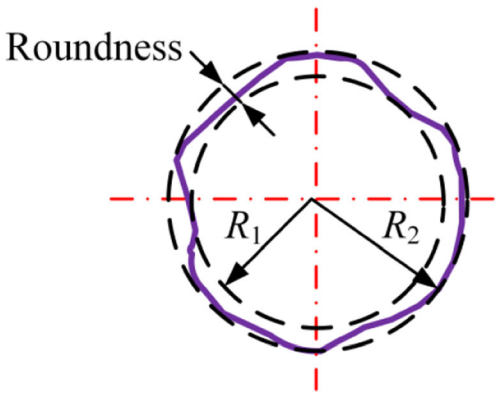


**Fig. 21** Schematic of roundness measurement

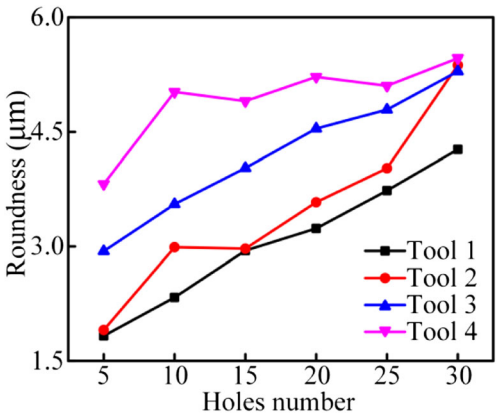


**Fig. 22** Roundness of micro-holes

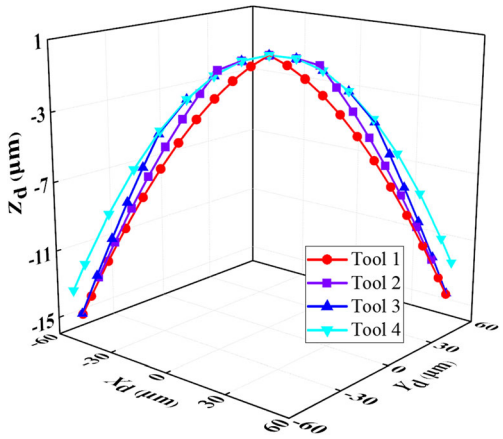


**Fig. 23** Cutting edge shapes of the micro-drills with thinned chisel edge

important role in the roundness of micro-holes. As the number of micro-holes increases, chisel edge and cutting edge wear become severe, leading to a larger roundness value.

With respect to hole quality, tool 1 ($l_1 = 0$ μm) is considered as the optimal helical point micro-drill with a thinned chisel edge. However, with respect to thrust force and tool wear, tool 2 ($l_1 = 42$ μm) is regarded as the optimal helical point micro-drill with a thinned chisel edge. The apparent chip curl and greater number of small-size chips produced using tool 2 ($l_1 = 42$ μm) facilitate chip movement. Thus, with the selected parameter range, the optimal micro-drill is tool 2 with a thinned chisel edge length of 42 μm.

## 5 Conclusions

This study evaluates the effect of chisel edge thinning in helical point micro-drills on the micro-drilling performance of stainless steel. Based on the mathematical models of the helical point micro-drill, the rake angle, lip inclination angle, uncut chip thickness, uncut chip width, and cutting edge shape of micro-drills with thinned chisel edge are calculated with the MATLAB software. Four kinds of helical point micro-drills, each with a thinned chisel edge of a distinct length, are fabricated using a six-axis computer numerical control (CNC) grinding machine. Micro-drilling experiments on 304 austenitic stainless steel are conducted. By discussing chip morphology, thrust force, drill wear, and micro-hole quality, several conclusions are summarized as follows:

1. During the drilling process, chip curl occurs and becomes more noticeable with an increase in chisel edge length; micro-drills with thinned chisel edges can improve chip breaking, causing more small-size chips generated than that of regular micro-drill.
2. The thrust force grows linearly with an increase in feed per tooth and number of holes. Also, it increases significantly with an increase in the chisel edge length. The reason is that the chisel edge with a negative rake angle replaces the inner cutting edge with a positive rake angle to squeeze the workpiece. However, the thrust force of tool 1 ($l_1 = 0$ μm) is slightly greater than that of tool 2 ($l_1 = 42$ μm), which is attributed to the increase in uncut chip width.
3. Drill tip wear is apparent for the four types of micro-drills. Moreover, the drill tip wear of tool 1 ($l_1 = 0$ μm), tool 2 ($l_1 = 42$ μm), and tool 3 ($l_1 = 84$ μm) is less than that of tool 4 ($l_1 = 140$ μm), and the workpiece material sticks to the chisel edge of tool 4 ($l_1 = 140$ μm). The inner cutting edge wear of tool 2 ($l_1 = 42$ μm) has the least area because of a smaller thrust force.
4. As the number of micro-holes increases, the shape accuracy at the micro-hole entrance gradually decreases. Compared with tool 4 ($l_1 = 140$ μm) which produces more entrance burrs, tool 1 ($l_1 = 0$ μm), tool 2 ($l_1 = 42$ μm), and tool 3 ($l_1 = 84$ μm) produce micro-holes with small entrance burrs and regular shapes. The roundness of the micro-holes gradually increases with an increase in the chisel edge length.

**Funding information** This work was supported by the National Natural Science Foundation of China (No. 51575049), National Basic Research Program of China (No. 2015CB059900), and Key Laboratory of Microsystems and Micro-structures Manufacturing of Ministry of Education, Harbin Institute of Technology (No. 2015KM005).



## References

1. Zhang SY, Liang ZQ, Wang XB, Zhou TF, Jiao L, Yan P, Jian HC (2016) Grinding process of helical micro-drill using a six-axis CNC grinding machine and its fundamental drilling performance. Int J Adv Manuf Technol 86(9–12):1–13
2. Çiçek A, Kıvak T, Samtaş G (2012) Application of Taguchi method for surface roughness and roundness error in drilling of AISI 316 stainless steel. Strojniski Vestnik 58(3):165–174
3. Ghany KA, Newishy M (2005) Cutting of 1.2mm thick austenitic stainless steel sheet using pulsed and CW Nd:YAG laser. Journal of Materials Processing 168(3):438–447
4. Armarego EJA, Wright JD (1984) Predictive models for drilling thrust and torque — a comparison of three flank configurations. CIRP Annals-Manufacturing Technology 33(1):5–10
5. Radhakrishnan T, Wu SM, Lin C (1983) A mathematical model for split point drill flanks. Journal of Engineering for Industry 105(3): 137–142
6. Fuh KH, Chen WC (1995) Cutting performance of thick web drills with curved primary cutting edges. Int J Mach Tools Manuf 35(7): 975–991
7. Beer N, Özkaya E, Biermann D (2014) Drilling of Inconel 718 with geometry-modified twist drills. Procedia Cirp 24:49–55
8. Wang J, Zhang Q (2008) A study of high-performance plane rake faced twist drills: part I: geometrical analysis and experimental investigation. Int J Mach Tools Manuf 48(11):1276–1285

9. Wang X, Zheng XH, An QL, Chen M (2012) Experimental investigation on drilling pcb through-holes. Adv Mater Res 426:56–59
10. Kato H, Nakata S, Ikenaga N (2007) Improvement of chip evacuation in drilling of lead-free brass using micro drill. Int J Autom Technol 8:874–879
11. Nanbu Y, Ochiai K, Ehara K, Matsuda S (2010) High-aspect-ratio microdrilling of the nozzle for gas turbine(2nd Report): effect of thinning of microdrill and ultrasonic vibration. Proceedings of JSPE Semestrial Meeting (Vol.2010, pp. 1017–1018). The Japan Society for Precis Eng.
12. Nanbu Y, Ochiai K, Horio K (2011) Influence on rake angle of chisel edge in high-aspect-ratio microdrilling. Journal of the Japan Society for Precision Engineering 77:713–717
13. Lin PD, Tzeng CS (2007) New method for determination of the pose of the grinding wheel for thinning drill points. Int J Mach Tools Manuf 47(15):2218–2229
14. Lin C, Kang SK, Ehmann KF (1995) Helical micro-drill point design and grinding. Journal of Engineering for Industry 117(3):277
15. Kang SK, Lin C, Ehmann KF (1993) Comparative analysis of planar and helical micro-drill points. Trans NAMRI/SME XXI:189–196
16. Liang ZQ, Jian HC, Wang XB, Zhao WX, Zhang SY, Yusuke O, Xue SY (2014) A 5-axis coordinated CNC grinding method for the flank of a non-coaxial helical micro-drill with the cylinder grinding wheel. Adv Mater Res 1017:654–659
17. Yan L, Jiang F (2013) A practical optimization design of helical geometry drill point and its grinding process. Int J Adv Manuf Technol 64(9–12):1387–1394
18. Zhang SY, Wang XB, Liang ZQ, Zhou TF, Jiao L, Yan P (2017) Modeling and optimization of the flute profile of micro-drill. Int J Adv Manuf Technol 1–14.